Mode-I, mode-II and mixed-mode I+II fracture behavior of composite bonded joints: Experimental characterization and numerical simulation

I. Floros[1], K.I. Tserpes[1,*] and T. Löbel[2]

[1]*Laboratory of Technology & Strength of Materials*
Department of Mechanical Engineering & Aeronautics
University of Patras, Patras, 26500, Greece

[2]*DLR, German Aerospace Center, Lilienthalplatz 7, 38108 Braunschweig, Germany*

Abstract:

The fracture behavior of composite bonded joints subjected to mode-I, mode-II and mixed-mode I+II loading conditions was characterized by mechanical testing and numerical simulation. The composite adherents were bonded using two different epoxy adhesives; namely, the EA 9695 film adhesive and the mixed EA 9395-EA 9396 paste adhesive. The fracture toughness of the joints was evaluated in terms of the critical energy release rate. Mode-I tests were conducted using the double-cantilever beam specimen, mode-II tests using the end-notch flexure specimen and mixed-mode tests (three mixity ratios) using a combination of the two aforementioned specimens. The fracture behavior of the bonded joints was also simulated using the cohesive zone modeling method aiming to evaluate the method and point out its strengths and weaknesses. The simulations were performed using the explicit FE code LS-DYNA. The experimental results show a considerable scatter which is common for fracture toughness tests. The joints assembled with the film adhesive have much larger fracture toughness (by 30-60%) than the joints with the paste adhesive, which exhibited a rather brittle behavior. The simulation results revealed that the cohesive zone modeling method performs well for mode-I load-cases while for mode-II and mixed-mode load-cases, modifications of the input parameters and the traction-separation law are needed in order for the method to effectively simulate the fracture behavior of the joints.

Keywords:

A. Polymer-matrix composites (PMCs); B. Fracture toughness; B. Debonding; C. Finite element analysis (FEA); D. Mechanical testing.

[*]Corresponding author. Tel. +30-2610-997498, Fax: +30-2610-997190, E-mail: kit2005@mech.upatras.gr

1. Introduction

In recent years, adhesive bonding finds an increasing use in aircraft structures both for assembling structural parts and applying composite patch repairs due to its specific advantages over mechanical fastening [1-3]. Nonetheless, joining and patch-repairing of large primary composite structural parts by adhesive bonding is for the moment not feasible due to several reasons such as the sensitivity of the bondline to bonding quality reduction scenarios [4-6], the inability of existing non-destructive testing techniques to detect weak bonds [4-6] and mainly, the failure of existing designs to comply with certification rules [7]. As the mechanically fastened interfaces in composite thin-walled structures induce a significant weight and cost penalty and mitigate the technical and economic benefits expected from the massive introduction of composites in aircrafts and the number of in-service patch repairs is increasing rapidly, due to the increasing number of in-service ageing aircrafts, there is a need to overcome the previously mentioned hindrances and enable the use of (boltless) adhesive bonding in primary large aircraft structures.

In general, strength of bonded joints is measured in terms of fracture toughness. Thus, both mechanical tests and numerical models aim at the development of functions between the applied force and crack growth in the adhesive.

Until today the mechanical tests used to measure the fracture toughness of bonded joints usually followed standards developed for characterizing interlaminar fracture toughness of composite laminates as only recently standards were published for bonded joints (ISO 25217 standard for mode-I testing). Despite the similarities between the two failure mechanisms, the debonding process is a far more complicated phenomenon than delamination as it takes place in a three-materials system (adherent, adhesive and adherent/adhesive interface) compared to delamination which takes place in a two-materials system (layers and interface between them). Thus, the standards often fail to accurately describe the fracture behavior of composites bonded joints.

In the literature, there have been reported several experimental works on fracture behavior of composite bonded joints e.g. [8-12]. The majority of them have focused on the mode-I loading as it is considered to be the most critical. However, this is not the case as during operation mixed-mode I+II loads of varying mixity are usually applied to composite bonded joints. It is therefore very important to characterize also the mode-II and mixed-mode I+II fracture behaviors of each composite adherent/adhesive system. To the author's knowledge, there have been reported very few works in which a complete characterization of the fracture behavior (mode-I, mode-II and mixed-mode I+II) of a composite adherent/adhesive system to have been performed e.g. [13].

Two fracture mechanics-based numerical approaches have been mainly used for simulating fracture behavior of composite bonded joints: the Cohesive Zone Modeling (CZM) method and the Virtual Crack Closure Technique (VCCT). Both approaches have strengths and weaknesses. The strengths of CZM are the capability of predicting initiation and growth of debonding without prior assumptions about location and direction and its applicability to complex structures subjected to complex loads. Its weaknesses are the difficulties to characterize the required input data and the mesh dependency. On the other hand, the strengths of the VCCT are the maturity, which comes from the numerous applications of the method in metals, and the direct growth prediction using the energy release rate *G*. Its weaknesses are the assumptions that need to be made for the cracks (number, location, size) and the difficulty in the application to complex structures subjected to complex loads. Although numerous works have been reported in the literature on the use of the CZM method e.g. [14-19] and the VCCT e.g. [20-23] for simulating crack growth in composite bonded joints, a complete assessment of the approaches is not feasible since the simulations have been performed for a single loading-mode, which in most cases is mode-I.

The aim of the present work is to fully characterize the fracture behavior of two different adhesive/composite adherent systems, that are widely used in aeronautic applications, by conducting mode-I, mode-II and mixed-mode I+II mechanical tests and to evaluate the CZM method through its critical application in the three loading modes.

2. Experimental

2.1 Materials and manufacturing

All CFRP plates consisted of 16 unidirectional plies of the 8552/IM7 Hexply prepreg material. A quasi-isotropic stacking sequence of $[0/+45/90/-45/0/+45/90/-45]_s$ with 0° surface plies was chosen to minimize the undesired delamination failure close to the bondline while testing. The autoclave curing cycle was performed in accordance with the material data sheet specifications leading to an overall plate thickness of 2 mm. A PTFE release film between the plate's surface and the steel tooling ensured a constant overall surface finish.

After cleaning with acetone and isopropanol, atmospheric plasma was used for surface treatment of the bonding surface (Plasmatreat generator FG5001) with the following parameters: plasma frequency 17 kHz, rotating nozzle (RD1004), velocity of 100 mm/s and a surface distance of 10 mm. For intermediate storage, activated surfaces were protected with aluminum foil.

A release film of 60 mm length was inserted at one site of all plates prior bonding to obtain an initial delamination for fracture toughness tests.

Two types of adhesive were used for bonding: a one-component epoxy film adhesive of high curing temperature (130°C) with an average thickness of 0.15 mm (Hysol EA9695 0.05 PSF K), which was cured in an autoclave cycle with a pressure of 4.5 bar and a temperature of 130°C applied for 2 hours, and a mixture of two paste adhesive systems (80 % Loctite EA9395 and 20 % Loctite EA9396). The latter is the unfilled version of the first adhesive; thus, chemical miscibility was ensured. By mixing the paste adhesives, an optimized viscosity for the specific application was attained. A high speed centrifugal mixer was used to obtain a homogenous mixture free of pores. The adhesive was applied by use of a cartridge. Metallic distances were implemented at the edges (trim area) of the plates to set the bondline thickness to its desired value of 0.3 mm. Subsequently, joining and curing of the mixed adhesive was performed in a heated press by applying a pressure of 3 bar and a temperature of 100°C for 2 hours.

All bonded plates were checked for porosities by ultrasonic C-scans. Afterwards, the plates were trimmed and cut to the final specimen dimensions specified by the standards of the tests.

2.2 Mechanical testing

Mode-I, mode-II and mixed-mode I+II tests of three mixity ratios were conducted to fully characterize the fracture toughness of the CFRP bonded joints in terms of critical energy release rate *G*. Mode-I and mixed-mode tests were conducted using a Tinius Olsen H5K-S UTM tensile machine with a load cell of 500 N while mode-II tests using an MTS universal testing machine with a load capacity of 100 kN.

2.2.1 Mode-I tests

Mode-I tests were conducted according to the ASTM 5528-01 standard [24] using the double cantilever beam (DCB) specimen schematically shown in Fig.1. The tests were conducted under the displacement rate of 1 mm/min. Fig.2 illustrates a specimen mounted on the tensile machine during a mode-I test. Crack growth was monitored at one side of the specimen since observations taken from first tests showed a symmetric crack growth for both adhesives.

The mode-I critical energy release rate G_{IC} was computed using the corrected beam theory (CBT) [24] and the Simple Beam Theory (SBT) [24]. According to the CBT theory, the critical energy release rate G_{IC} is given by

$$G_{IC} = \frac{3P\delta}{2b(a + |\Delta|)} F \quad (J/m^2) \tag{1}$$

where P is the force at crack initiation, δ is the cross-head displacement at crack initiation, b is the specimen's width, a is the total debonding length, Δ is a correction factor derived experimentally from the plot of the cube root of the compliance, $(\delta/P)^{1/3}$ and F is the large displacement multiplication factor given by

$$F = 1 - \frac{3}{10}\left(\frac{\delta}{a}\right)^2 - \frac{3}{2}\left(\frac{\delta t}{a^2}\right) \tag{2}$$

where t is the half the sum of half thickness of piano hinges and half thickness of the adherent (see Fig.A1.1 in [24]).

The CBT theory is used in cases of stable crack growth. In cases of unstable crack growth ('stick-slip'), the SBT theory is used instead. According to the SBT theory, G_{IC} is given by

$$G_{IC} = \frac{4P^2}{E_s b^2}\left(\frac{3a^2}{h^3} + \frac{1}{h}\right) \quad (J/m^2) \tag{3}$$

where P, a and b are the same as in Eq.(1), E_S is the independently-measured tensile modulus of the substrate (68.22 GPa) and h is the thickness of one adherent.

2.2.2 Mode-II tests

Mode-II tests were conducted according to the AITM1-0006 standard [25] using the end-notch flexure (ENF) specimen schematically shown in Fig.3. As this a three-point bending test, no tabs were mounted on the specimens. The tests were conducted under a displacement rate of 1 mm/min. Fig.4 illustrates a specimen mounted on the tensile machine during a mode-II test.

G_{IIC} was derived at crack initiation [25] by

$$G_{IIC} = \frac{9 \times P \times a_{ini}^2 \times \delta \times 1000}{2 \times b \times (1/4\, L^3 + 3a_{ini}^3)} \quad (J/m^2) \tag{4}$$

where P is force at crack initiation, a_{ini} is the initial crack of the specimen, b is the specimen's width, L is the span length (see Fig.3) and δ is the cross-head displacement at crack initiation.

2.3.2 Mixed mode tests

Mixed-mode I+II tests were conducted according to the ASTM 6671-06 standard [26] using a combination of the DCB and ENF specimens. The mixed-mode loading conditions were applied using the Mixed-Mode Bending (MMB) test apparatus manufactured for this purpose [26]. The schematic of the MMB test apparatus is shown in Fig.5. The tests were conducted under a displacement rate of 1 mm/min. Fig.6 illustrates a specimen mounted on MMB test apparatus during a mixed-mode test. In order to fully characterize the mixed-mode fracture toughness of the CFRP bonded joints, three mixed-mode ratios $G_{IIC}/(G_{IC}+G_{IIC})$ were used, namely 0.2, 0.6 and 0.85.

The mixed-mode critical energy release rate G was evaluated according to the following procedure [26]. The lever of the length c to produce the desired mode-mixture G_{II}/G was derived by

$$c=\frac{12\beta^2+3\alpha+8\beta\sqrt{3\alpha}}{36\beta^2-3\alpha}L \tag{5}$$

where α is the mode mixture transformation parameter for setting the lever length, β is the non-dimensional crack length correction parameter for mode-mixture and L is the half-span length of the MMB test apparatus (Fig.5). The parameters α and β were derived from

$$\alpha=\frac{1-\frac{G_{II}}{G}}{\frac{G_{II}}{G}} \tag{6}$$

$$\beta=\frac{\alpha+\chi h}{\alpha+0.42\chi h}, \tag{7}$$

respectively, where χ is the crack length correction parameter given by

$$\chi\equiv\sqrt{\frac{E_{11}}{11G_{13}}\left\{3-2\left(\frac{\Gamma}{1+\Gamma}\right)^2\right\}} \tag{8}$$

where Γ is the transverse modulus correction parameter derived as

$$\Gamma \equiv 1.18\frac{\sqrt{E_{11}E_{22}}}{G_{13}} \tag{9}$$

where E_{11}, E_{22} G_{13} are the longitudinal modulus of elasticity measured in tension, the transverse modulus of elasticity and the out-of-plane shear modulus of the adherent, respectively.

A calibration specimen made from steel was used to calculate the bending modulus of the MMB apparatus. The compliance of the calibration specimen is given by

$$C_{cal} = \frac{2L(c+L)^2}{E_{cal}b_{cal}t^3} \tag{10}$$

where b_{cal} and t are the width and thickness of the calibration specimen, respectively and E_{cal} is the modulus of calibration bar. In the calibration process, the MMB apparatus is loaded to approximately 75% of the estimated force of the tests and the slope m_{cal} of the force-displacement curve is measured. The compliance of the MMB test system C_{sys} is calculated by

$$C_{sys} = \frac{1}{m_{cal}} - C_{cal} \tag{11}$$

where m_{cal} is the slope of calibration curve. The specimen was mounted on the MMB apparatus and loaded until the debonding to exceed the 25 mm. Then, the MMB apparatus was unloaded and the bending modulus E_{If} was calculated using

$$E_{If} = \frac{8(a_0+\chi h)^3(3c-L)^2 + [6(\alpha_0+0.42\chi h)^3 + 4L^3](c+L)^2}{16L^2bh^3\left(\frac{1}{m} - C_{sys}\right)} \tag{12}$$

where a_{ini} is the initial debonding length, h and b are the half thickness and width of the specimen, respectively, and m is the slope of the force displacement curve.

The mode-I G_I and mode-II G_{II} components of the strain energy release rate and the total energy release rate G were calculated by

$$G_I = \frac{12P^2(3c-L)^2}{16b^2h^3L^2E_{If}}(a+\chi h)^2 \tag{13}$$

$$G_{II} = \frac{9P^2(c+L)^2}{16b^2h^3L^2E_{If}}(a+0.42\chi h)^2 \tag{14}$$

$$G = G_I + G_{II}, \tag{15}$$

respectively, where P is the critical force to start the crack and a is the total debonding length. When the applied force P is associated with the start of the crack (P_c), the total strain energy release rate equals to the fracture toughness (G_c).

3. Numerical simulation

3.1 The CZM method

The fracture behavior of the composite bonded joints was simulated using the Cohesive Zone Modeling (CZM) method. This method has been widely used in the last decade for simulating delamination progression in composite materials and debonding progression in bonded joints mainly due to its ease of use as it has been implemented into many commercial FE codes. However, the CZM has several drawbacks and often fails to reproduce the experimental results due to the weakness of the theory involved and the difficulty to determine with accuracy the required input parameters. In this work, the CZM has been evaluated through its application to the joints with the film adhesive for mode-I, mode-II and mixed-mode loading conditions.

The CZM method was implemented using the LS-DYNA explicit FE code [27]. This choice was based on previous experience with the implicit ANSYS FE code which revealed convergence problems in some mode-II dominated problems. For the analysis, the linear elastic/linear softening (bilinear) traction-separation law was adopted. Fig.7 shows the bilinear constitutive model in tension for mode-I. The region until point 1 is the elastic part of the material response. Until then material has not suffered any damage and the unloading at this point would follow the elastic line. The region from point 1 to point 2 represents the material softening (damage growth) area. Once the loading has progressed beyond point 2 the material has suffered some damage (damage parameter is greater than zero, but less than one), but the adherents have not been separated yet. At point 2 the adherents separate permanently (damage parameter has reached unity). The total area under the triangle (points 0, 1, 2) represents the

energy it takes to debond the adherents and is known as the fracture energy. In LS-DYNA [27], the fracture energy is an input parameter. It has units of energy/area. In addition, the elastic stiffness (slope) and the peak stress (point 1) are required for complete definition of the bilinear law. Numerical studies have shown that the fracture toughness has to be accurate, but the initial stiffness and the peak stress do not need to be accurate, i.e. they can be changed without affecting the overall results. Camanho and Davila [28] use a constant value 10E+6 for all materials and call it "penalty stiffness". The same value has been used also in the present model. Then, in order to keep the fracture toughness (area under the triangle) correct, the peak stress has to be adjusted accordingly.

The constitutive law described in Fig.7 is for tension loading and separation of the adherents in the normal direction. The mixed-mode behavior is described by the mixed-mode bilinear traction shown in Fig.8. The ultimate displacements in the normal and tangential directions are the displacements at the time when the material has failed completely, i.e., the tractions are zero. The linear stiffness for loading followed by the linear softening during the damage provides an especially simple relationship between the energy release rates, the peak tractions, and the ultimate displacements:

$$G_{IC} = T \cdot \delta_I^F / 2 \tag{16}$$

$$G_{IIC} = S \cdot \delta_{II}^F / 2 \tag{17}$$

The subscripts I and II refer to the normal and shear, as before, and the subscript C refers to "critical". The critical values are input to LS-DYNA [27]. The ratio G_I/G_{IC} is the ratio of the shaded triangle to the whole triangle in Fig.8. If the peak tractions are not specified, they are computed from the ultimate displacements.

In this cohesive material model, the total mixed-mode relative displacement $\delta_m = \sqrt{\delta_I^2 + \delta_{II}^2}$ where $\delta_1 = \delta_3$ is the separation in normal direction (mode-I) and $\delta_{II} = \sqrt{\delta_1^2 + \delta_2^2}$ is the separation in tangential direction (mode-II). The mixed-mode damage initiation displacement δ^0 (onset of softening) is given by

$$\delta^0 = \delta_I^0 \delta_{II}^0 \sqrt{\frac{1 + \beta^2}{(\delta_{II}^0)^2 + (\beta \delta_I^0)^2}} \tag{18}$$

where $\delta_I^0 = T/E_n$ ($E_n$is the stiffness normal to the plane of the cohesive element) and $\delta_{II}^0 = S/E_t$ (E_t is the stiffness in the plane of the cohesive element) are the single mode damage initiation separations and $\beta = \frac{\delta_{II}}{\delta_I}$ is the mode mixity. The ultimate mixed-mode displacement (total failure) for the power B-K law [30] is:

$$\delta^F = \frac{2}{\delta^0\left(\frac{1}{1+\beta^2}E_n + \frac{\beta}{1+\beta^2}E_t\right)}\left[G_{IC} + (G_{IIC} - G_{IC})\left(\frac{\beta^2 E_t}{E_n + \beta^2 E_t}\right)^2\right] \tag{19}$$

3.2 Progressive damage modeling

For simulating damage in the composite adherents, which could be developed at the mode-II and mode-II dominated mixed-mode load-cases due to high bending loads, the progressive damage modeling method was adopted. To this end, the material model MAT161 of the LS-DYNA was used. The specific material model implements automatically the progressive damage modeling method by combining a set of strain-based Hashin-type failure criteria for predicting tension/shear fiber failure, compression fiber failure, perpendicular matrix failure and delamination and a damage mechanics property degradation module for simulating the damage effects. Theoretical details, which are neglected here for the sake of briefness, as well as an evaluation of the method, can be found in [27].

3.3 FE model

In the FE model of the mode-I specimen, the composite adherents were modeled using the Element Formulation (ELFORM) 2 which refers to a fully integrated 8-noded solid element with 3 DOFs per node. For the element an orthotropic elastic behavior was considered. The mode-I load was modeled by applying incremental normal displacements at the rows of the nodes located at the position of the piano hinges.

In the FE model of the mode-II specimen, the composite adherents were modeled using the ELFORM 1 which refers to a constant stress 8-noded solid element with 3 DOFs per node. For the element an enhanced composite damage behavior was considered. For the numerical application of the mode-II load model, the experimental apparatus was modeled; two cylindrical shells were modeled for supporting the specimen and a solid cylinder for applying the load. Between the three cylinders and the specimen, contact was modeled using the AUTOMATIC_SURFACE_TO_SURFACE contact option of the LS-DYNA [27]. The same contact option was also used for modeling contact between the two adherents

at the area of the pre-crack that occurs due to bending. The FE mesh of the specimen and the three cylinders is shown in Fig.9.

In the FE model of the mixed-mode specimen, the composite adherents were modeled using the ELFORM 2 option. For the element an enhanced composite damage behavior was considered. The mixed-mode load was applied in the model through two supports: a pin at one specimen's end and a hinge at the other end, and two normal forces: a force applied downwards at the center of the specimen and a force applied upwards at the hinge-supported end of the specimen. The forces were derived according to the methodology described in [29]. Again, contact was modeled between the two adherents at the area of the pre-crack using the AUTOMATIC_SURFACE_TO_SURFACE option [27].

In all cases, the adhesive was modeled using ELFORM 19 which is an 8-noded cohesive element with 3 DOFs per node.

4. Results and discussion

The experimental and numerical results on the fracture behavior of the CFRP joints will be presented in parallel for each loading mode in order to evaluate the predictive capability of the of the CZM model and emphasize the dependence of the model on experiments.

4.1 Mode-I

In Fig.10 the experimental force-displacement curves for the mode-I load-case of the bonded joints assembled using the EA 9695 film adhesive are plotted. The curves show a considerable scatter, especially in the maximum force, which is mainly attributed to the initial (small) part of a larger slope of the curves; the larger this part is the larger is the maximum force. One specimen (05) showed a stable crack growth and four specimens a mixed stable-unstable crack growth. The computed G_{IC} values of the specimens are listed in Table 1. The G_{IC} values of all specimens were evaluated using the CBT method (Eq.(1)) by excluding the unstable part of the curve. For all specimens with the EA 9695 adhesive tested in mode-I, a cohesive failure mode was observed. Fig.11a illustrates the failure surfaces of a specimen with a stable crack growth while Fig.11b a photo of the failure surfaces of the specimens with the mixed stable-unstable crack growth.

In Fig.12 the experimental force-displacement curves of the mode-I tests of the bonded joints assembled using the mixed EA 9395-EA 9396 adhesive are plotted. The curves show a considerable scatter which is related to the initial part of larger slope as in the case of the EA 9695 adhesive. All five specimens showed an unstable crack growth. The G_{IC} values of the specimens, all computed using the

SBT theory (Eq.(3)), are also listed in Table 1. For all mode-I tests with the mixed adhesive, a cohesive failure mode, as shown in Fig.11c, was observed.

In Fig.10 the numerical force-displacement curve has been added. The curve was predicted using the properties listed in Table 2. The values of G_{IC} and G_{IIC} are the mean experimental values of (see Table 1); the other properties were obtained from the literature for the EA 9695 adhesive. The numerical curve compares very well with the experimental curves in terms of stiffness, maximum force and crack growth. This finding validates the capability of the CZM to accurately describe the mode-I fracture behavior of bonded joints. On the other hand, the CZM is not capable to simulate the unstable crack growth that takes place in the case of the mixed (EA 9395-EA 9396) paste adhesive. In this case, the predicted crack growth curve is expected to pass close to the peaks of the experimental unstable crack growth curve.

4.2 Mode-II

In Fig.13 the experimental force-displacement curves of the mode-II tests of the bonded joints assembled using the EA 9695 adhesive are plotted. The curves show an almost linear behavior of the specimens up to the applied displacement of 6.5-7.0 mm. From that point, matrix cracking started to accumulate at the adherents until final failure of the specimens (maximum load) which was due to fiber failure of the outer layers of the adherent in compression. Crack initiation at the adhesive occurred around 500 N without reducing the bending stiffness of the specimens due to the relatively low thickness of the adhesive compared to the thickness of the adherents. The G_{IIC} values of the specimens, listed in Table 1, were computed using Eq.(4). All joints failed in an adhesive failure mode as can be seen in Fig.14a.

The same comments stand more or less for the mode-II fracture behavior of the bonded joints assembled using the mixed EA 9395-EA 9396 adhesive described by the load-displacement curves depicted in Fig.15. The only difference is that the joints with the mixed adhesive failed in a cohesive failure mode as can be seen in Fig.14b.

In Fig.13 the numerical force-displacement curve has been also added. For the mode-II load-case, the joint with the mixed adhesive was not modeled as it presents a similar mode-II behavior with the EA 9695 adhesive. The input parameters to the model are listed in Table 2. As can be seen, the CZM predicted accurately the force at crack initiation. However, contrary to the tests, crack initiation reduced significantly the bending stiffness of the model. The smaller bending stiffness led to larger strains which caused premature failure as the failure criteria used in the PDM are based on strain. This discrepancy is attributed to the fact that in the CZM debonding corresponds to a decrease in the model's thickness by

a value equal to adhesive's thickness, which is not the case in the tests. Nevertheless, a similar decrease in bending stiffness due to the crack initiation in the adhesive is expected to occur also in joints with thinner adherents.

4.3 Mixed-mode

In Figs 16 and 17, the force-displacement curves of the mixed-mode tests of mixity ratio of 0.2 of the joints with the film and paste adhesive are plotted, respectively. In both cases, the joints showed a linear response up to the maximum load at which the crack propagated suddenly up to the desired length. A similar response was observed for all joints of both adhesives tested under mixed-mode loading conditions (for the tests with ratios of 0.6 and 0.85 only the *G* values are listed in Table 1). The differences between the two adhesives and between the different mixity ratios are at the maximum load, the displacement at crack growth and the failure modes. The G values for all mixed-mode tests are listed in Table 1, the failure modes are listed in Table 3, together with the failure modes of all tests conducted, and photos of the failure surfaces are illustrated in Fig.18.

In Fig.16 two numerical force-displacement curves have been also added: the initial curve computed using the parameters used also for mode-I and mode-II simulations and a curve computed from a calibration process aimed to approach the crack initiation point. The initial and calibrated parameters are listed in Table 2. In this case, the initial numerical curve initially followed the experimental curve and at the load of 40 N started to deviate showing a decreasing slope. From that point, the behavior of some of the cohesive elements inserted the softening part of the traction-separation due to the small peak traction, T in normal direction stress used (8.3 MPa). With increasing the T, the numerical curve started to approach the force-displacement curve. The curve with T =50 MPa falls within the experimental range. The deviation between the initial value of T and the one reproduced the experiments is an indication of how much higher is the local T used by the CZM method compared to the experimentally derived global strength of the material. Although the calibrated numerical curve describes well the crack initiation, it fails completely to describe the sudden debonding propagation. This inability is attributed to the softening part of the bilinear traction-separation law. In order for the CZM method to be able to describe sudden crack growth phenomena a traction-separation law with a modified softening part must be adopted.

4.4 Comparison between the film and paste adhesive

By comparing the force-displacement curves and the values of *G* in Table 1, it is concluded that the film adhesive EA 9695 exhibits a much greater fracture toughness than the paste EA 9395-EA 9396 adhesive.

The difference in *G* ranges from 30 to 60%. In addition, as revealed from the unstable crack growth behavior under mode-I loading, the paste adhesive is much more brittle than the film adhesive.

5. Conclusions

In this work, the mode-I, mode-II and mixed-mode I+II fracture behaviors of two different composite adherent/adhesive systems were fully characterized by mechanical testing and the CZM method was evaluated through simulations performed for some of the loading cases. From the experimental and numerical results obtained the following conclusions can be drawn:

- The experimental results show a considerable scatter which is common for fracture toughness tests. The joints with film adhesive show much larger fracture toughness (by 30-60%) than the joints with the paste adhesive, which exhibited a rather brittle behavior.
- Under mode-I load conditions, the film adhesive exhibited a stable crack growth contrary to the paste adhesive which exhibited an unstable crack growth. Both types of joints failed under the desired failure cohesive mode. For this case, the CZM method simulated very well the fracture behavior of the joints.
- Under mode-II loading conditions, the crack initiation, occurred at 25% of the maximum load, did not change the slope of the force-displacement curve due to relatively high thickness of the adherents. The joints with the film adhesive failed under an adhesive/mixed failure/delamination failure mode while the joints with the paste adhesive under a cohesive failure mode. The CZM method predicted accurately the crack initiation; however, it failed to predict the maximum force due to the significant change in the slope of the numerical curve.
- Under mixed-mode loading conditions, both joints showed a linear behavior until sudden crack growth to the desired length. Different failure modes were observed for the different mixity ratios. Compared to the pure mode-I and mode-II load-cases, fiber-tear failure mode was also observed. The CZM method failed to predict crack initiation, mainly due to the deviation between the actual local material properties and the averaged global experimental values used. Moreover, the bilinear traction-separation law failed to capture the sudden crack growth behavior.
- In general, it is concluded that the CZM method works well in mode-I load-cases. In mode-II and mixed-mode load-cases, where the fracture behavior is more complex, modifications in the local material properties and the traction-separation law are needed in order for the method to give accurate predictions.

Acknowledgement

The research leading to these results has received funding from the European Union Seventh Framework Programme (FP7/2007-2013) under grant agreement n° 314180 (Project BOPACS: Boltless Assembling of Primary Aerospace Composite Structures).

References

[1]. Banea MD, Da Silva LFM. Adhesively bonded joints in composite materials: an overview. Proc Inst Mech Eng, Part L: J Mater Des Appl 2009;223:1

[2]. Adams RD. Adhesive bonding: science, technology and applications. Woodhead Publishing; 2005.

[3]. Da Silva LFM, Öchsner A. Modeling of adhesive bonded joints. Berlin: Springer; 2008.

[4]. Markatos DN, Tserpes KI, Rau E, Markus S, Ehrhart B, Pantelakis Sp. The effects of manufacturing-induced and in-service related bonding quality reduction on the mode-I fracture toughness of composite bonded joints for aeronautical use. Composites Part B: Engineering 2013;45(1):556-564.

[5]. Markatos DN, Tserpes KI, Rau E, Brune K, Pantelakis Sp. Degradation of mode-I fracture toughness of CFRP bonded joints due to release agent and moisture pre-bond contamination. Journal of Adhesion. 2013;90(2):156-173.

[6]. Tserpes KI, Markatos DN, Brune K, Hoffmann M, Rau E, Pantelakis Sp. A detailed experimental study of the effects of pre-bond contamination with a hydraulic fluid, thermal degradation, and poor curing on fracture toughness of composite bonded joints. Journal of Adhesion Science and Technology 2014;28(18):1865-1880.

[7]. Boltless Joining of Primary Aerospace Composite Structures (BOPACS). Description of Work, 2012.

[8]. Katsiropoulos CV, Chamos AN, Tserpes KI, Pantelakis SG. Fracture toughness and shear behavior of composite bonded joints based on a novel aerospace adhesive Composites Part B: Engineering 43;(2):240-248.

[9]. Gefu J, Zhenyu Q, Guoqiang L. Effects of bondline thickness on Mode-I nonlinear interfacial fracture of laminated composites: An experimental study. Composites: Part B 47;2013:1–7.

[10]. Mohan J, Ivanković A, Murphy N. Mode I fracture toughness of co-cured and secondary bonded composite joints. International Journal of Adhesion and Adhesives 2014;51:13-22.

[11]. Zhang Y, Vassilopoulos AP, Keller T. Mode I and II fracture behavior of adhesively-bonded pultruded composite joints. Engineering Fracture Mechanics 2010;77:128-143.

[12]. Ashcroft IA, Hughes DJ, Shaw SJ. Mode I fracture of epoxy bonded composite joints: 1. Quasi-static loading. International Journal of Adhesion and Adhesives 2001;21:87-99.

[13]. Blackman BRK, Kinloch AJ, Rodriguez-Sanchez FS, Teo WS. The fracture behaviour of adhesively-bonded composite joints: Effects of rate of test and mode of loading. International Journal of Solids and Structures. 2012;49:1434-1452.

[14]. Gang L, Chun L. Assessment of debond simulation and cohesive zone length in a bonded composite joint. Composites: Part B 2015;69:359-368.

[15]. de Moura MFSF, Gonçalves JPM. Development of a cohesive zone model for fatigue/fracture characterization of composite bonded joints under mode II loading. International Journal of

Adhesion and Adhesives 2014;54:224-230.
[16]. Li S, Thouless MD, Waas AM, Schroeder JA, Zavattieri PD. Mixed-mode cohesive-zone models for fracture of an adhesively bonded polymer–matrix composite. Engineering Fracture Mechanics 2006;73:64-78.
[17]. Fernandes RMRP, Chousal JAG, de Moura MFSF, Xavier J. Determination of cohesive laws of composite bonded joints under mode II loading. Composites Part B: Engineering 2013;52:269-274.
[18]. Li S, Thouless MD, Waas AM, Schroeder JA, Zavattieri PD. Use of mode-I cohesive-zone models to describe the fracture of an adhesively-bonded polymer-matrix composite. Composites Science and Technology 2005;65:281-293.
[19]. Tserpes KI, Koumpias AS. Comparison between a Cohesive Zone Model and a Continuum Damage Model in Predicting Mode-I Fracture Behavior of Adhesively Bonded Joints. Computer Modeling in Engineering & Sciences (CMES) 2012;83:169-181.
[20]. Das RR, Pradhan B. Adhesion failure analyses of bonded tubular single lap joints in laminated fibre reinforced plastic composites. International Journal of Adhesion & Adhesives 2010;30:425-438.
[21]. Goh JY, Georgiadis S, Orifici AC, Wang CH. Effects of bondline flaws on the damage tolerance of composite scarf Joints Composites: Part A 2013;55:110-119.
[22]. Mohammadreza, K., Mehrabadi, FA. Fracture analysis in adhesive composite material/aluminum joints under mode-I loading; experimental and numerical approaches. International Journal of Adhesion and Adhesives 2012;39:8-14
[23]. Zhang Y, Vassilopoulos AP, Keller T. Mixed-mode fracture of adhesively-bonded pultruded composite lap joints. Engineering Fracture Mechanics 2010;77:2712-2726.
[24]. ASTM D5528-01, Standard Test Method for Mode I Interlaminar Fracture Toughness of Unidirectional Fiber-Reinforced Polymer Matrix Composites , ASTM International, West Conshohocken, PA, 2001
[25]. AITM1-1.0006, Airbus test method: determination of fracture toughness energy of CFRP bonded joints – mode II; 2006.
[26]. ASTM D6671 / D6671M-06, Standard Test Method for Mixed Mode I-Mode II Interlaminar Fracture Toughness of Unidirectional Fiber Reinforced Polymer Matrix Composites, ASTM International, West Conshohocken, PA, 2006.
[27]. LS-DYNA Theory Manual. Livermore Software Technology Corporation, CA, USA, 2014.
[28]. Camanho PP, Dávila CG. Mixed-mode decohesion finite elements for the simulation of delamination in composite materials. NASA-Technical paper 2002;211737:1.
[29]. Reeder JR and Crews JR. Mixed-Mode Bending Method for Delamination Testing, AIAA Journal 1990;28:1270–1276.
[30]. Benzeggagh ML and Kenane M. Measurement of Mixed-Mode Delamination Fracture Toughness of Unidirectional Glass/Epoxy Composites with Mixed-Mode Bending Apparatus. Composites Science and Technology 1996;56:439-449.

Captions to figures:

Fig.1: Schematic representation and dimensions of the DCB specimen

Fig.2: Photo of a specimen during a mode-I test

Fig.3: Schematic representation and dimensions of the ENF specimen

Fig.4: Photo of a specimen during a mode-II test

Fig.5: Schematic representation and dimensions of the MMB apparatus [26]

Fig.6: Photo of a specimen during a mixed-mode test

Fig.7: Schematic representation of the bilinear traction-separation law for the mode-I load-case

Fig.8: Schematic representation of the bilinear traction-separation law for the mixed-mode load-case

Fig.9: FE mesh of the specimen and cylinders for the mode-II load-case

Fig.10: Experimental and numerical force-displacement curves of the EA 9695 bonded joints loaded in mode-I

Fig.11: Photos of failure surfaces of specimens loaded in mode-I: a. EA 9695 specimen with stable crack growth, b. EA 9695 specimen with unstable crack growth and c. EA 9395-EA 9396 specimen

Figh.12: Experimental force-displacement curves of the EA 9395- EA 9396 bonded joints loaded in mode-I

Fig.13: Experimental and numerical force-displacement curves of the EA 9695 bonded joints loaded in mode-II

Fig.14: Photos of failure surfaces of specimens loaded in mode-II: a. EA 9695 specimen and b. EA 9395-EA 9396 specimen.

Fig.15: Experimental force-displacement curves of the EA 9395-EA 9396 bonded joints loaded in mode-II

Fig.16: Experimental and numerical force-displacement curves of the EA 9695 bonded joints loaded in mixed-mode $(G_{II}/G = 0.2)$

Fig.17: Experimental force-displacement curves of the EA 9395-EA 9396 bonded joints loaded in mixed-mode $(G_{II}/G = 0.2)$

Fig.18: Photos of failure surfaces of specimens loaded in mixed-mode$(G_{II}/G = 0.2)$: a. EA 9695 specimen and b. EA 9395-EA 9396 specimen.

Captions to Tables:

Table 1: Experimental *G* values

Table 2: Parameters used in the CZM simulations

Table 3: List of failure modes

Fig.1

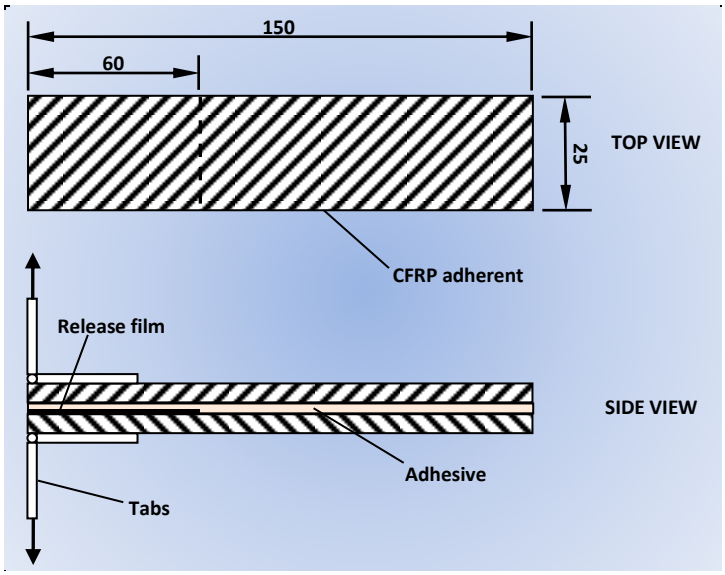
150
60
25
TOP VIEW
CFRP adherent
Release film
SIDE VIEW
Adhesive
Tabs

Fig.2

Fig.3

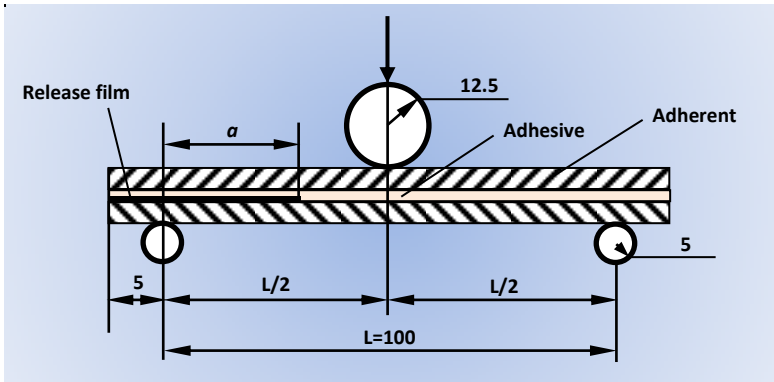

Fig.4

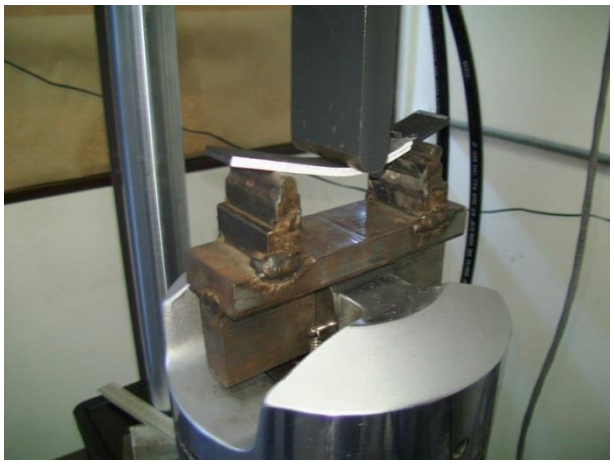

Fig.5

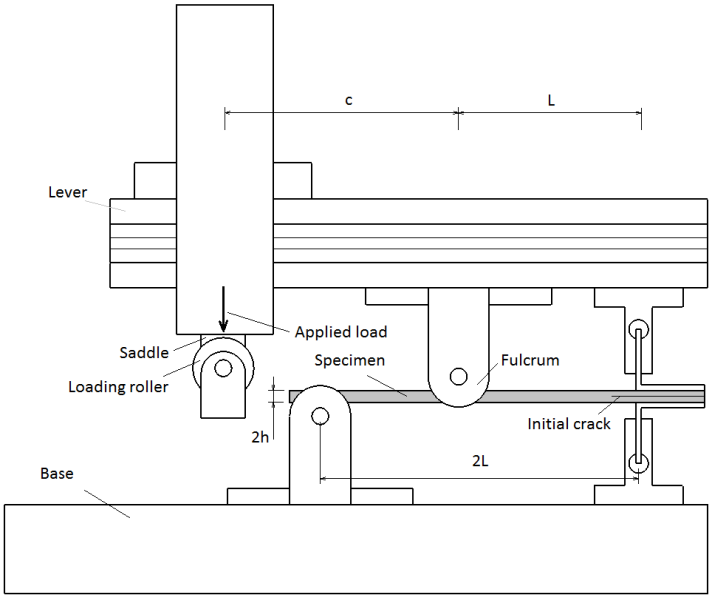
c
L
Lever
Applied load
Saddle
Specimen
Fulcrum
Loading roller
Initial crack
2h
2L
Base

Fig.6

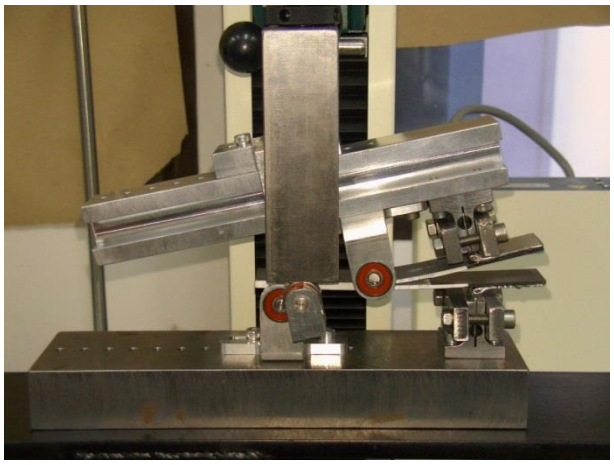

Fig.7

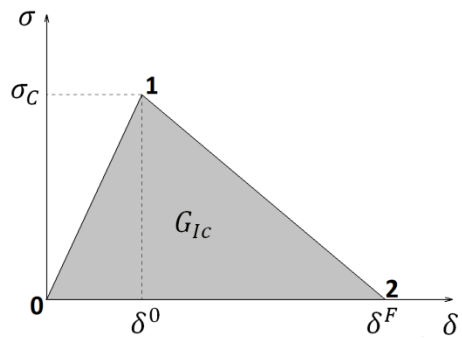

Fig.8

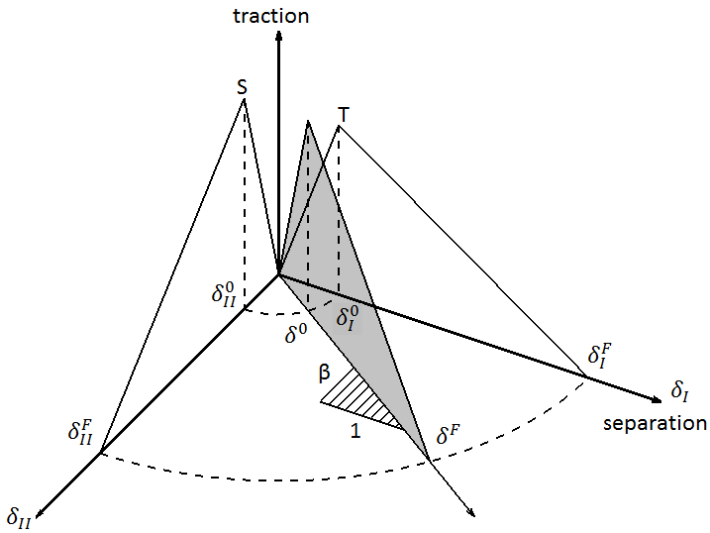
traction
S
T
δ_{II}^0
δ^0
δ_I^0
δ_I^F
δ_I
separation
β
1
δ^F
δ_{II}^F
δ_{II}

Fig.9

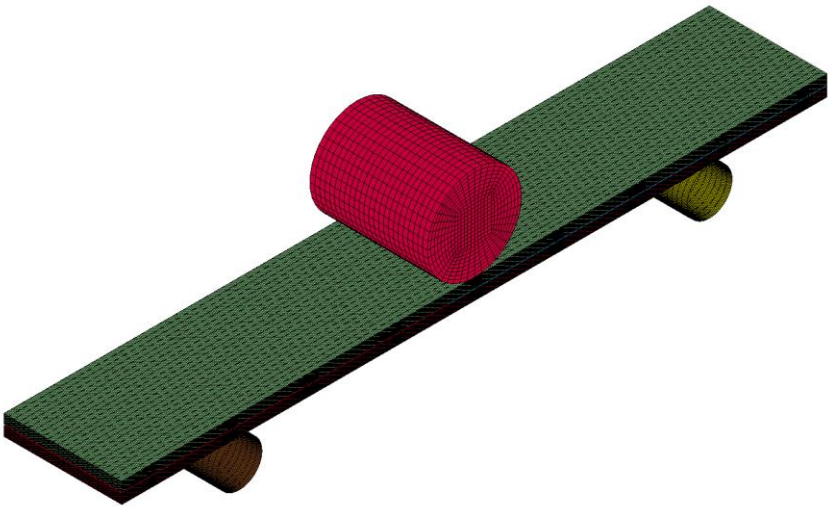

Fig.10

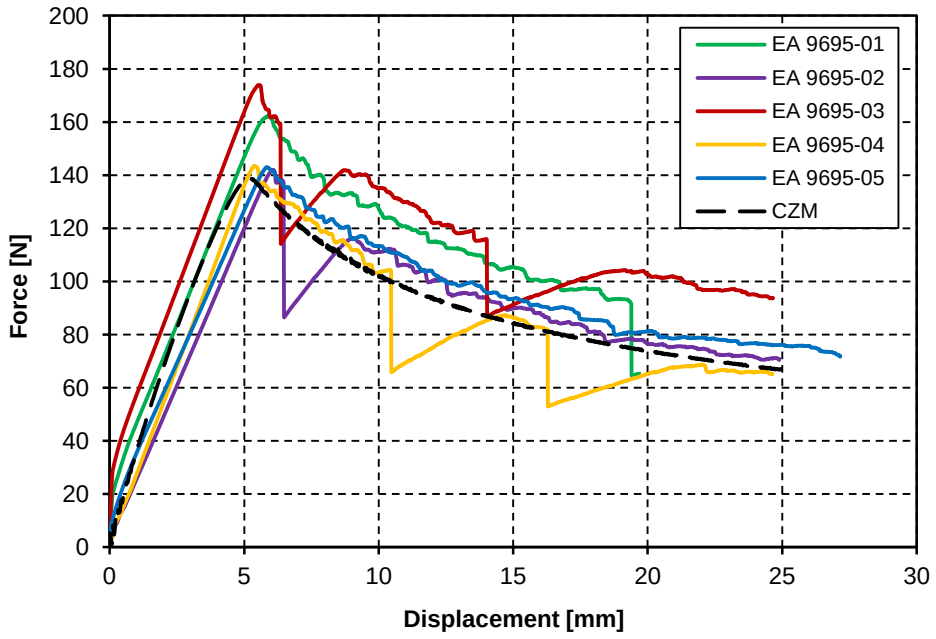
200
180
160
140
120
100
80
60
40
20
0
Force [N]
0
5
10
15
20
25
30
Displacement [mm]
EA 9695-01
EA 9695-02
EA 9695-03
EA 9695-04
EA 9695-05
CZM

Fig.11

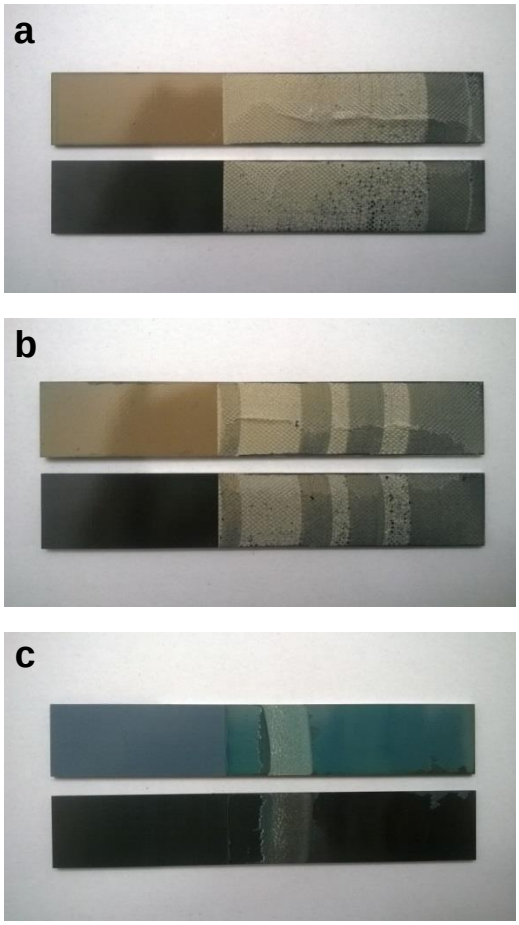

Fig.12

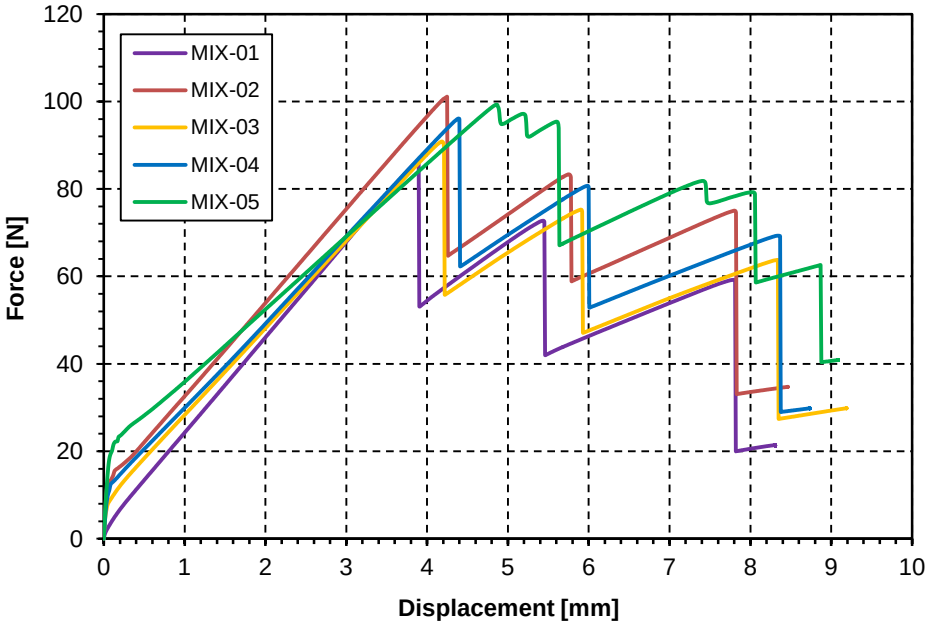
MIX-01
MIX-02
MIX-03
MIX-04
MIX-05
Force [N]
Displacement [mm]
0
20
40
60
80
100
120
0
1
2
3
4
5
6
7
8
9
10

Fig.13

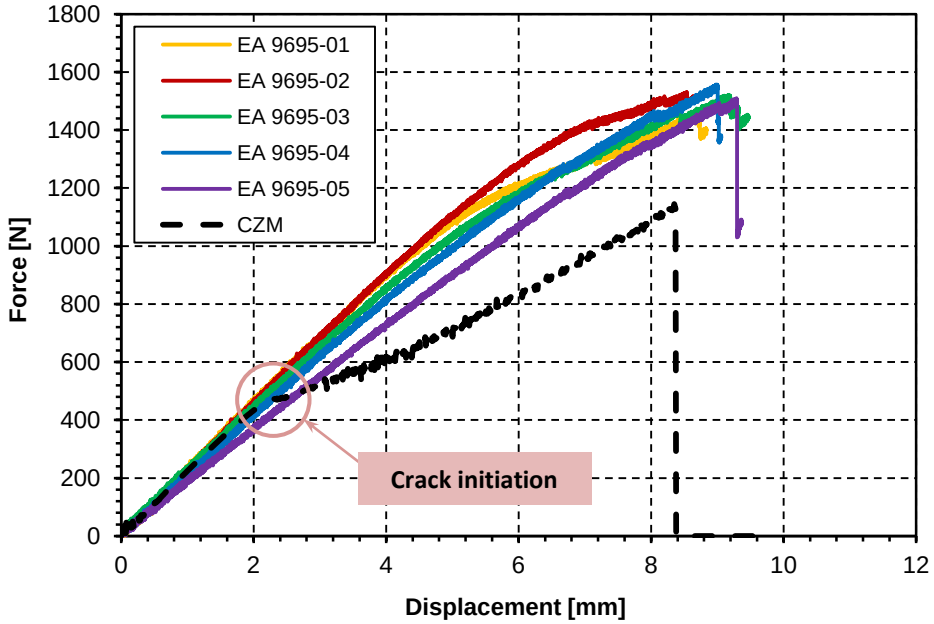
1800
1600
1400
1200
1000
800
600
400
200
0
Force [N]
0
2
4
6
8
10
12
Displacement [mm]
EA 9695-01
EA 9695-02
EA 9695-03
EA 9695-04
EA 9695-05
CZM
Crack initiation

Fig.14

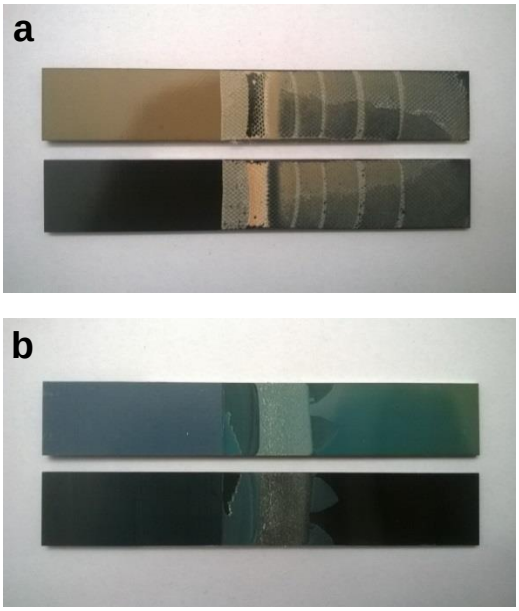

Fig.15

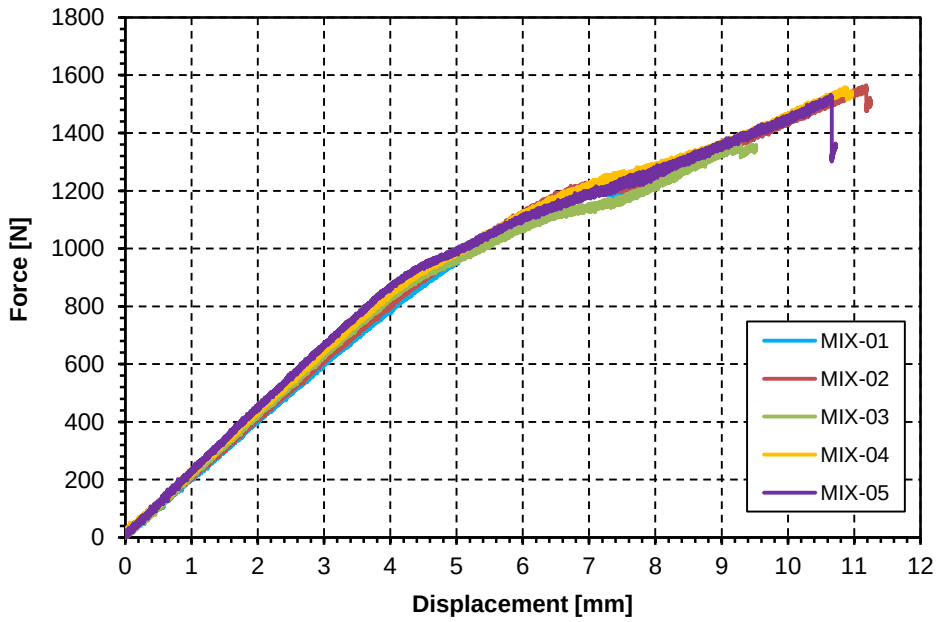
1800
1600
1400
1200
1000
800
600
400
200
0
Force [N]
0
1
2
3
4
5
6
7
8
9
10
11
12
Displacement [mm]
MIX-01
MIX-02
MIX-03
MIX-04
MIX-05

Fig.16

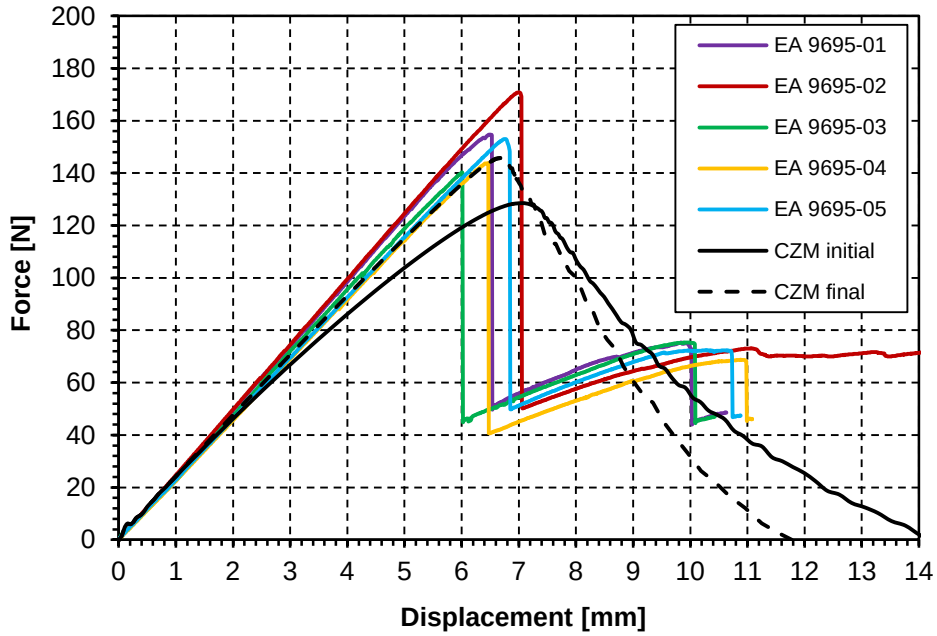
Force [N]
Displacement [mm]
0
20
40
60
80
100
120
140
160
180
200
0
1
2
3
4
5
6
7
8
9
10
11
12
13
14
EA 9695-01
EA 9695-02
EA 9695-03
EA 9695-04
EA 9695-05
CZM initial
CZM final

Fig.17

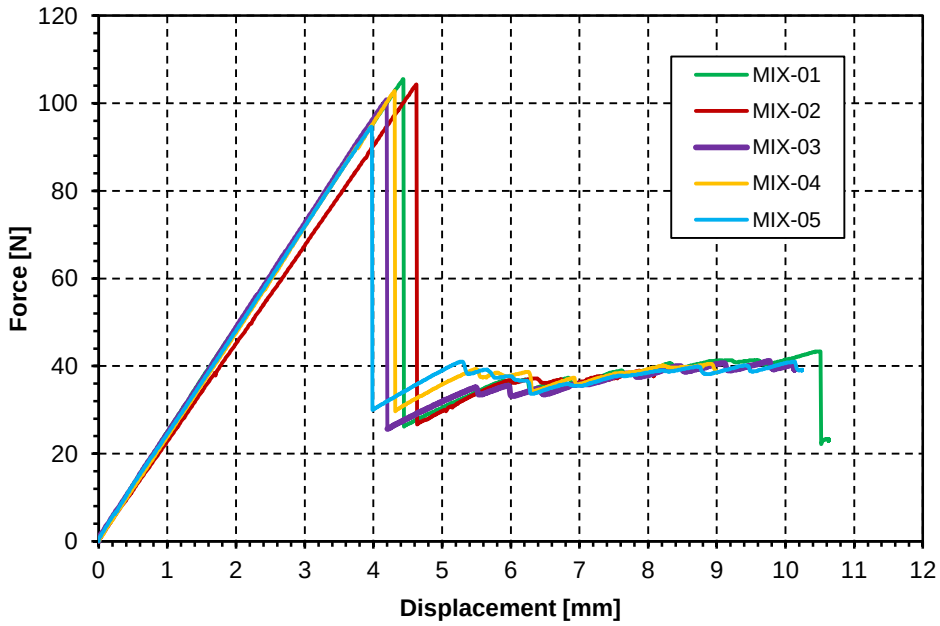
120
100
80
60
40
20
0
Force [N]
0
1
2
3
4
5
6
7
8
9
10
11
12
Displacement [mm]
MIX-01
MIX-02
MIX-03
MIX-04
MIX-05

Fig.18

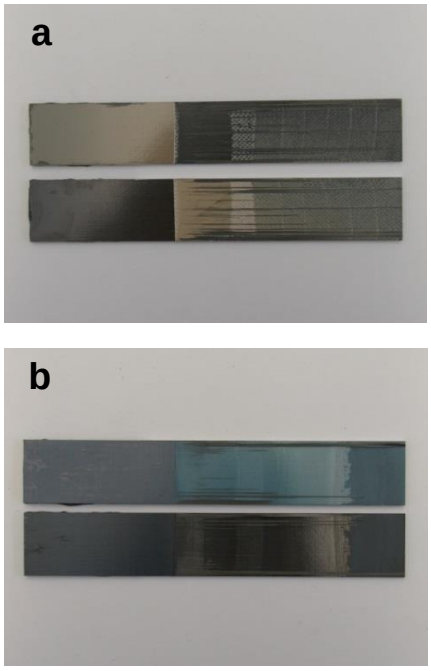

Table 1

	G values (J/m²)				
Specimen	Mode-I	Mode-II	Mixed-mode ($G_{II}/G = 0.2$)	Mixed-mode ($G_{II}/G = 0.6$)	Mixed-mode ($G_{II}/G = 0.85$)
EA9695-01	1107.60	759.56	903.32	1784.36	3251.53
EA9695-02	995.05	654.03	1114.92	1329.91	3921.78
EA9695-03	1034.37	1289.91	793.32	1971.59	3614.71
EA9695-04	998.95	974.66	873.99	1378.10	3338.10
EA9695-05	956.64	238.88	993.33	1570.04	3109.58
Mean (standard deviation)	1018.52 (56.89)	783.41 (389.53)	935.78 (98.44)	1606.80 (108.61)	3447.14 (48.46)
MIX-01	318.10	353.80	462.34	809.75	1824.14
MIX-02	302.05	347.84	478.58	1031.76	1696.64
MIX-03	308.83	526.28	414. 84	933.36	1817.16
MIX-04	298.39	700.16	432.51	1080.18	1436.60
MIX-05	423.13	529.11	370.24	970.72	1499.85
Mean (standard deviation)	330.10 (52.54)	491.44 (146.42)	431.63 (33.97)	965.15 (41.41)	1654.88 (26.88)

Table 2

Load-case	Model parameter	Value
Mode-I	Peak traction in normal direction	8.3 MPa
	Peak traction in tangential direction	34.5 MPa
	Ultimate displacement in normal direction	0.246 mm
	Ultimate displacement in tangential direction	0.045 mm
	G_{IC}	1.019 N/mm
	G_{IIC}	0.783 N/mm
Mode-II	Peak traction in normal direction	8.3 MPa
	Peak traction in tangential direction	34.5 MPa
	Ultimate displacement in normal direction	0.246 mm
	Ultimate displacement in tangential direction	0.015 mm
	G_{IC}	1.019 N/mm
	G_{IIC}	0.783 N/mm
Mixed-mode ($G_{II}/G = 0.2$)	Peak traction in normal direction	8.3 MPa / 50 MPa
	Peak traction in tangential direction	34.5 MPa
	Ultimate displacement in normal direction	0.246 mm
	Ultimate displacement in tangential direction	0.045 mm
	G_{IC}	1.019 N/mm / 1.3 N/mm
	G_{IIC}	0.783 N/mm

Table 3

	Failure mode				
Bonded joint	Mode-I	Mode-II	Mixed-mode ($G_{II}/G = 0.2$)	Mixed-mode ($G_{II}/G = 0.6$)	Mixed-mode ($G_{II}/G = 0.85$)
EA 9695	Cohesive	Adhesive/mixed failure/delamination	Fiber-tear	Adhesive	Light fiber-tear
MIX	Cohesive	Cohesive	Fiber-tear	Fiber-tear	Light fiber-tear